ARTICLE
PUBLISHED ONLINE: 11 JULY 2016 | DOI: 10.1038/NCHEMBIO.2125
nature chemical biology

Pistol ribozyme adopts a pseudoknot fold facilitating site-specific in-line cleavage

Aiming Ren[1,2,5], Nikola Vušurović[3–5], Jennifer Gebetsberger[3,4], Pu Gao[2], Michael Juen[3,4], Christoph Kreutz[3,4], Ronald Micura[3,4]* & Dinshaw J Patel[2]*

The field of small self-cleaving nucleolytic ribozymes has been invigorated by the recent discovery of the twister, twister-sister, pistol and hatchet ribozymes. We report the crystal structure of a pistol ribozyme termed env25, which adopts a compact tertiary architecture stabilized by an embedded pseudoknot fold. The G-U cleavage site adopts a splayed-apart conformation with in-line alignment of the modeled 2′-O of G for attack on the adjacent to-be-cleaved P-O5′ bond. Highly conserved residues G40 (N1 position) and A32 (N3 and 2′-OH positions) are aligned to act as a general base and a general acid, respectively, to accelerate cleavage chemistry, with their roles confirmed by cleavage assays on variants, and an increased pK_a of 4.7 for A32. Our structure of the pistol ribozyme defined how the overall and local topologies dictate the in-line alignment at the G-U cleavage site, with cleavage assays on variants revealing key residues that participate in acid-base-catalyzed cleavage chemistry.

Small self-cleaving ribozymes are widely distributed in nature[1,2] and are essential for rolling-circle-based replication of satellite and pathogenic RNAs[3,4] and processing of repetitive RNA species[5]. Members of this nucleolytic ribozyme class include hammerhead[6,7], hairpin[8,9], glmS[10], hepatitis delta[11,12] and Varkud satellite[5,13] ribozymes, which mediate cleavage chemistry through nucleobase-specific acid-base catalysis. X-ray structural studies on the hammerhead[14], hairpin[15,16], glmS[17,18], HDV[19,20] and Varkud satellite[21] ribozymes have defined the role of hydrogen-bond networks, ionic and hydrophobic interactions for generation of catalytic pockets, which capitalize on steric constraints to generate in-line cleavage alignments involving attack of the 2′-OH on the adjacent 3′ phosphate and general acid-base chemistry to catalyze site-specific cleavage of the phosphodiester backbone[1,22–25]. Key challenges relate to which RNA residues contribute to ribozyme-mediated rate enhancement through involvement in nucleophilic activation of the 2′-OH and protonation of the P-O5′ oxygen at the cleavage step, as well as what factors contribute to stabilization of the transition state. Additional insights have emerged into how the transition state (vanadate mimics) can be preferentially accommodated in the catalytic pocket, though there remains uncertainty regarding the role of divalent cations in mediating cleavage chemistry.

The recent discovery of twister, twister sister, pistol and hatchet self-cleaving ribozymes by comparative genomic analysis[2,26] has opened a unique opportunity to undertake structure-function studies to comparatively assess the architectural diversity, catalytic cores and mechanism of action of these four small self-cleaving ribozymes. To this end, recent chemical[26], structural[27–29], biochemical[26,30] and computational[31] studies have provided insights into the topological constraints contributing to catalysis by the twister ribozyme.

A recent study has reported a small self-cleaving ribozyme composed of three stems, a hairpin and an internal loop, named the pistol ribozyme (**Fig. 1a**)[2,32]. Highly conserved nucleotides are primarily located in the internal loop and the linker segment (AAA trinucleotide), whereas segments of the hairpin and internal loops are predicted to be involved in 5-base-pair pseudoknot formation[2]. Cleavage occurs at a modestly conserved G-U dinucleotide junctional site, whose length is strictly conserved. RNA cleavage has been shown to be dependent on Mg^{2+} and the cleavage rate had increased with increasing pH. Studies using phosphorothioate substitution at the cleavage site suggest that the pistol ribozyme exploits a contact involving one of two nonbridging phosphate oxygens to facilitate catalysis. RNA-strand scission occurs with a rate constant of up to 10 min^{-1} under physiological pH and in the presence of Mg^{2+} (ref. 32).

To our knowledge, there had been no indications of either the tertiary fold of the pistol ribozyme, or which residues line the catalytic pocket, to facilitate cleavage at the G-U site within the short arm of the internal loop (**Fig. 1a**). Of particular interest was whether the conserved AAA trinucleotide has the potential to form stacked A-minor triples with the minor groove of a duplex segment. Metal-ion dependence studies have been interpreted to conclude that the pistol ribozyme does not require inner-sphere coordination of a divalent cation for catalysis[32].

Here we report a structure-function study of the env25 pistol ribozyme. The structure defines a splayed-out orientation and in-line alignment of the internucleotide linkage at the G-U cleavage site, while also defining the relative alignment of nearby nucleotides and divalent cations with the potential for contributing to the catalytic mechanism. We monitored the cleavage propensity of structure-guided variants of the pistol ribozyme to deduce insights into the principles underlying site-specific cleavage chemistry. In addition, we capitalized on NMR spectroscopy site-specific labeling approaches to measure the pK_a of an adenine lining the catalytic pocket, and applied fluorescence-based approaches to measure precise cleavage rates as a function of temperature. Finally, we compared our structure of the env25 pistol ribozyme with a recent structure of the RzB hammerhead ribozyme.

RESULTS

Structure of the pistol ribozyme

There are ten highly conserved (>97% invariant) residues in the pistol ribozyme secondary structure (**Fig. 1a**)[2]. Our efforts focused on the env25 pistol ribozyme, whose sequence and secondary structure

[1]Life Sciences Institute, Zhejiang University, Hangzhou, China. [2]Structural Biology Program, Memorial Sloan-Kettering Cancer, New York, New York, USA. [3]Institute of Organic Chemistry, Leopold Franzens University, Innsbruck, Austria. [4]Center of Molecular Biosciences (CMBI), Innsbruck, Austria. [5]These authors contributed equally to this work. *e-mail: pateld@mskcc.org or ronald.micura@uibk.ac.at

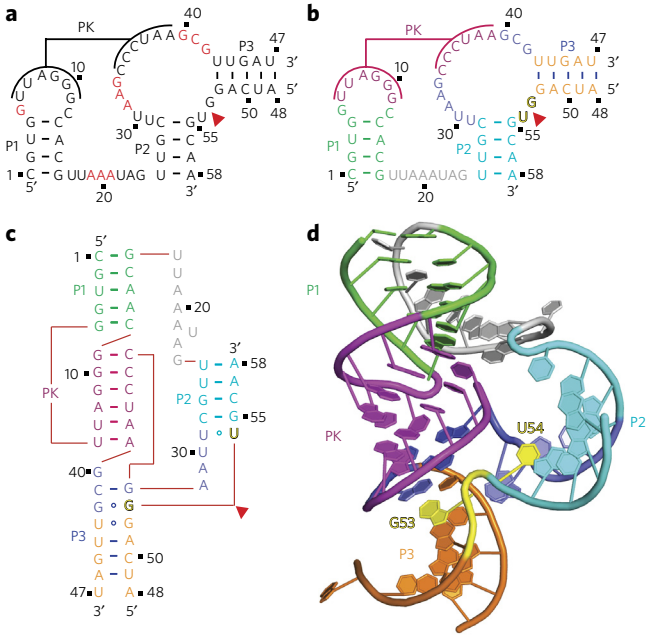

Figure 1 | Secondary and tertiary structure of the env25 pistol ribozyme. (**a**) Secondary structure of the env25 pistol ribozyme showing highly conserved residues in red (adapted from ref. 2). PK, proposed pseudoknot. In this two-strand construct, the longer ribozyme strand is labeled from 1 to 47, and the shorter substrate strand that contains the G53-U54 cleavage site is labeled from 48 to 58. (**b**) Color-coded representation of the secondary structure of the env25 pistol ribozyme. (**c**) Schematic of the folding topology based on the crystal structure of the env25 pistol ribozyme. (**d**) 2.7 Å structure of the pistol ribozyme, color-coded as in **b**, with the G53-U54 cleavage site in yellow.

are shown in **Figure 1b**. We generated the env25 pistol ribozyme by annealing two chemically synthesized strands, the shorter substrate strand is an 11-mer (residues 48–58) containing the G53-U54 cleavage site, and the longer ribozyme strand is a 47-mer (residues 1–47) (**Fig. 1b**). We synthetically incorporated dG53 in the substrate strand at the G–U site to prevent cleavage.

We solved the crystal structure of the bimolecular construct of the dG53-containing env25 pistol ribozyme at 2.7 Å resolution. The tertiary structural fold is shown schematically in **Figure 1c** and in a ribbon representation in **Figure 1d** (X-ray statistics listed in **Supplementary Results**, **Supplementary Table 1**). The crystals belonged to space group $P322_1$, with one molecule in each asymmetric unit.

We observed formation of a six-base-pair pseudoknot involving complementary loop segments between the hairpin and internal loops, as predicted previously[2], with the pseudoknot duplex positioned between stems P1 and P3 (**Fig. 1d**). There was continuous stacking of stem P3, a small segment involving noncanonical pairing interactions, pseudoknot stem and stem P1 (**Fig. 1d** and **Supplementary Fig. 1a**). Stem P2 folded back and was positioned opposite the pseudoknot stem, resulting in an overall compact fold, containing the splayed apart G53-U54 site (**Fig. 1d**).

Pairing alignment of conserved residues

The highly conserved A31-A32-G33 and G40-C41-G42 segments (**Fig. 1a**) together with G53 at the cleavage site of the pistol ribozyme were brought into proximity (**Fig. 2a**) as a result of pairing alignments involving G42 (**Fig. 2b**) and G40·(G33-C41) triple formation (**Fig. 2c**). Notably, the G40-C41 step formed an in-plane platform (**Fig. 2c**), whereas G40, which adopts a C2′-*endo* sugar pucker, was involved in a major-groove-aligned triple with the Watson-Crick G33-C41 pair (**Fig. 2c**), thereby anchoring it in place. The Watson-Crick edge of G42 was directed toward the sugar of A32 (**Fig. 2b**).

The A19-A20-A21 segment, which is also highly conserved in pistol ribozyme sequences[2] (**Fig. 1a**), was positioned in the minor groove of stem P1, where it formed consecutive A-minor triples (**Supplementary Fig. 1b**), with this stacked A-rich segment tilted with respect to the base pairs of stem P1 (**Fig. 2d**). Each adenine formed A-minor triples with adjacent base pairs of stem P1, as shown for A20 in **Figure 2e**.

The remaining highly conserved residue was G5, positioned adjacent to stem P1 (**Fig. 1a**,**b**) in the pistol ribozyme. Stem P1 was extended through formation of a Watson-Crick G5-C12 base pair, with G5 anchored in place through formation of a minor groove triple involving the sugar edge of G24 and the G5-C12 pair (**Supplementary Fig. 1c**).

In-line alignment at G53-U54 cleavage site

The G53-U54 internucleotide linkage targeted for hydrolysis adopted an extended splayed out conformation (**Fig. 3a**). G53 was maximally stacked between G40 and G52, whereas U54 was partially stacked between U30 and G55. Both G53 and U54 adopted *anti* alignments at their glycosidic bonds with sugar puckers adopting C2′-*endo* at G53 and C3′-*endo* at U54.

Our structure of the pistol ribozyme contained a deoxy sugar (2′-H) at G53 (dG53), so as to prevent cleavage at the G53-U54 site by an active ribozyme. Incorporation of dG52 could possibly contribute to its C2′-*endo* sugar pucker, a characteristic of deoxy sugars. After structure refinement, the 2′-H was replaced by 2′-OH at G53, to check for in-line alignment required for cleavage of the P-O5′ bond of the intervening phosphate at the G53-U54 site. The modeled 2′-OH structure exhibited a 2′-O (of G53) to P (at the G53-U54 site) distance of ~2.8 Å and a 2′-O (of G53) to P-O5′ angle (at G53-U54 site) of ~167° (**Fig. 3b**).

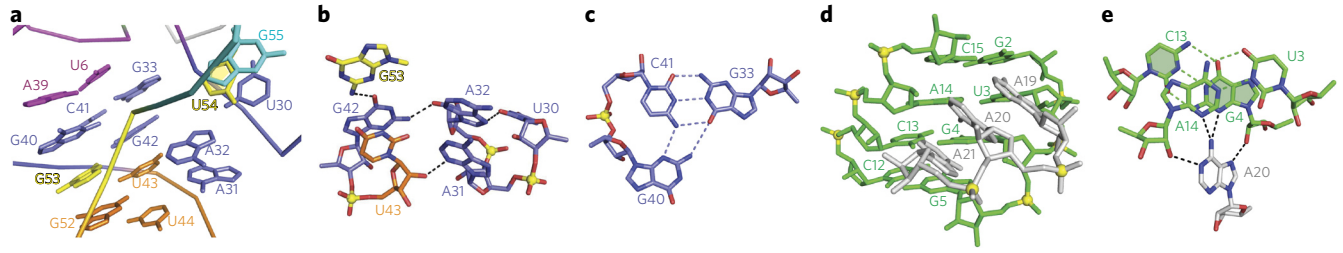

Figure 2 | Structural details of the env25 pistol ribozyme in the vicinity of the G53-U54 cleavage site. (**a**) Representation of bases surrounding the G53-U54 cleavage site, color coded as in **Figure 1b**,**c**. (**b**) Hydrogen bonding alignments involving the G42-U43, U30-A31-A32 and G53 segments. (**c**) The major groove-aligned G40•(G33-C41) triple involving highly conserved residues G40 and C41. Note the platform at the G40-C41 step. (**d**) Alignment of the highly conserved A19-A20-A21 segment within the minor groove of stem P1. The AAA segment is tilted relative to the base pairs of stem P1. (**e**) Bifurcated hydrogen binds between the Hoogsteen edge of A20 and the minor groove of adjacent base pairs of stem P1.

Bases and cations in vicinity of the cleavage site

Bases G40 and A32 were positioned close to the splayed apart G53-U54 cleavage site (**Fig. 3b**). The separation between the N1 of G40 and the modeled nucleophilic 2′-OH oxygen of G53 was ~3.4 Å. G40 was anchored in place through stacking (**Fig. 3b**) and also through formation of a base triple with the major groove of the G33-C41 pair (**Fig. 2c**). The bridging P-O5′ oxygen at the G53-U54 cleavage site was ~5.3 Å from the 2′-OH of A32 and ~5.0 Å from the N3 of A32 (**Fig. 3c**). These distances can be compared with their counterparts in the pH 8.0 structures of the RzB hammerhead ribozyme (Protein Data Bank (PDB) identifier 5DI2) (**Fig. 3d**).

We observed a bound hydrated Mg^{2+} ion in the vicinity of the G53-U54 cleavage site (**Supplementary Fig. 1d**), which we verified by soaking the crystal in Mn^{2+}-containing solution and collecting an anomalous data set (**Supplementary Fig. 1e**). The hydrated Mg^{2+} cation was coordinated directly to N7 of G33, but was not directly coordinated to neither of nonbridging phosphate oxygens (Mg^{2+}-O distances of 4.0 Å and 4.9 Å) of the G53-U54 site.

Mutations and cleavage activities

We performed cleavage assays of several single-mutation pistol variants using ion-exchange high-performance liquid chromatography (HPLC; **Fig. 4**). Under single-turnover conditions, wild-type env25 pistol ribozyme cleaved its substrate to completeness in less than 10 min (**Fig. 4a**). As anticipated, mutations of G40 and A32 that are closest to the cleavage site had substantial impact on the cleavage activities. Mutation of G40 to adenine completely abolished cleavage (**Fig. 4b**). We note that replacement of G40 by A would also disrupt the G40·(G33-C41) base triple (**Fig. 2c**). When we mutated A32 to cytosine, cleavage was completely abolished (**Fig. 4c**); we presume that replacement of the purine A by the smaller pyrimidine C alters the base heteroatom to O5′ separation, thereby impacting cleavage chemistry. By contrast, the A32U variant ribozyme had some activity, with about 50% yield after 45 min (**Supplementary Fig. 2c**), whereas the A32G variant ribozyme cleaved its substrate almost 100% in less than 10 min (**Supplementary Fig. 2d**).

To further test the role of A32 we investigated the A32dA variant, with this mutant showing only about 25% cleavage yield after 10 min and about 90% after 45 min (**Fig. 4d**). To learn more about a potential role of the N3 in dA32, we investigated the corresponding 3-deaza nucleoside. We observed no cleavage at all for the A32c^3dA variant after 45 min (**Fig. 4e**).

When we replaced the conserved AAA trinucleotide in the linker segment by UUU, we observed no cleavage after 10 min, with about 50% cleavage after 45 min (**Fig. 4f**). G42, which is positioned adjacent to the G53-U54 cleavage site has a key role, because compared to wild-type control (**Fig. 4g**), mutation of G42 to A was deleterious (**Fig. 4h**). Mutation of G42 to U also severely decreased activity (**Fig. 4i**).

NMR spectroscopy experiments: pK_a of A32

To better understand the participation of A32 in the mechanism of phosphodiester cleavage of pistol ribozymes, we used NMR spectroscopy to determine its pK_a value, as we have recently done for a twister ribozyme[30]. By solid-phase RNA synthesis, we prepared the same construct as that used for X-ray structure determination, but with a site-specifically ^{15}N-labeled uridine at position 26 and a ^{13}C2-labeled adenine at position 32 (**Fig. 5a**). Whereas the 11-nucleotide (nt) substrate strand displayed no ^{1}H imino proton signals, the 47-nt ribozyme strand was already partly prefolded under the no-added-Mg^{2+} buffer conditions used (**Fig. 5b**). Only in the presence of Mg^{2+}, the pseudoknot fold was completed, according to the increased number and distribution of resonances (**Fig. 5b**). When we added the substrate in the presence of Mg^2, additional signals confirmed complex formation (**Fig. 5b**) as did the appearance of a correlation in the ^{1}H–^{15}N HSQC spectrum of the ^{15}N-labeled U26 probe (**Supplementary Fig. 3a**) that senses P2 duplex formation with the substrate because of reduced imino proton exchange with the solvent. We observed the cross-peak in the typical chemical shift range of A-U base pairs, consistent with the formation of Watson-Crick base pairs in the ribozyme's substrate-binding arms (**Supplementary Fig. 3b**).

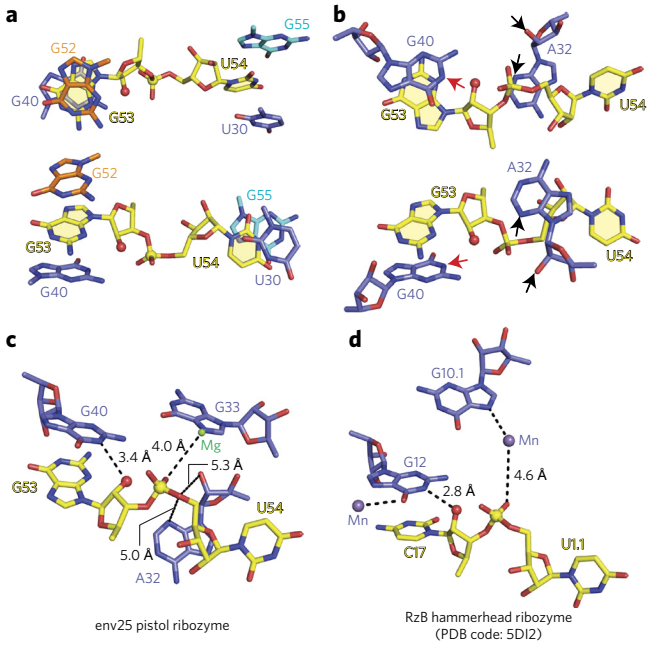

Figure 3 | In-line alignment at the G53-U54 cleavage site in the env25 pistol ribozyme and comparison with the structure of the RzB hammerhead ribozyme. (**a**) Base stacking with G53 (top) and U54 (bottom) at the G53-U54 cleavage site. The 2′-OH oxygen of G53 was modeled given that the pistol ribozyme construct contained dG53 to prevent cleavage. (**b**) Positioning of G40 and A32 in the proximity of the G53-U54 cleavage site. The N1 of G53 is labeled by a red arrow, and N3 and 2′-OH oxygen of A32 are labeled by black arrows. (**c**,**d**) Cleavage sites of the env25 pistol ribozyme (**c**) and RzB hammerhead ribozyme (PDB code: 5DI2) (**d**), emphasizing the conformation of the dinucleotide step at the cleavage site, alignment of adjacent nucleotides and divalent cations, as well as critical distances.

Next, we conducted pH-dependent NMR spectroscopy experiments with the ^{13}C2-A32 (**Supplementary Fig. 4a**) noncleavable ribozyme complex (containing dG53) to determine the pK_a of that adenine. In the $^1J(^1H,^{13}C)$ heteronuclear single quantum correlation (HSQC) spectra, we observed a very sharp, highly defined pH dependence of the A32 C2-^{13}C chemical shift with the transition between protonated and deprotonated forms (in slow exchange) in the pH 4.6 to 4.8 range, indicative of an estimated pK_a value of 4.7 (**Fig. 5c**). By contrast, we measured a pK_a in the 3.6 to 3.85 range for A in the duplex and single-strand context[33] (**Supplementary Fig. 4b,c**). The pK_a shifted by one pH unit toward neutrality for A32 in the pistol ribozyme.

Fluorescence assays: kinetics and conformational changes

We used a fluorescence-based, real-time cleavage assay[34,35] to monitor cleavage kinetics (**Fig. 6**). We integrated 2-aminopurine (Ap) (**Supplementary Fig. 5a**) into a base pair of stem P2 (A57Ap). Ap becomes stacked (and hence fluorescence-quenched) when this stem forms through substrate binding upon addition of Mg^{2+}. After cleavage, the 5-nt fragment (containing Ap) dissociates because of the rather weak remaining base-pairing interactions (**Fig. 6a**). This experimental setup resulted in the expected immediate fluorescence decrease upon Mg^{2+} addition (folding and annealing), followed by

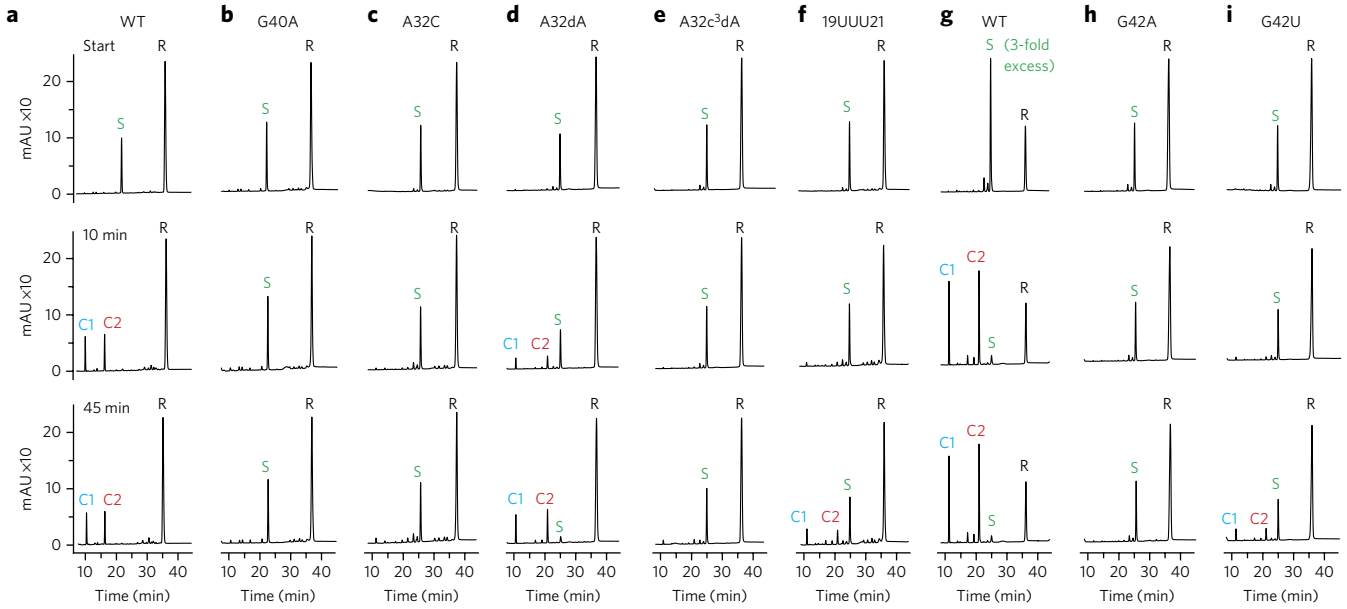

Figure 4 | Self-cleavage of the env25 pistol ribozyme. (**a**–**i**) For wild-type (WT) ribozyme and variants with indicated mutations, HPLC traces are depicted that represent the analysis of the start of the cleavage reaction (top) and indicated time points thereafter (middle and bottom) at 55 μM RNA concentration (single turnover conditions were used, except for **g** as highlighted); 2 mM $MgCl_2$, 100 mM KCl, 30 mM HEPES, pH 7.5, 23 °C. In **f**, 19UUU21 indicates A19U-A20U-A21U variant. R, 47-nt ribozyme, S, 11-nt substrate; C1 and C2, 6-nt and 5-nt cleavage products. HPLC conditions were Dionex DNAPac column (4 mm × 250 mm), 80 °C, 1 mL min^{-1}, 0–60% buffer B in 45 min. Buffer A: Tris–HCl (25 mM), urea (6 M), pH 8.0. Buffer B: Tris–HCl (25 mM), urea (6 M), $NaClO_4$ (0.5 M), pH 8.0.

an increase that we attributed to the release of the cleaved pentamer (**Fig. 6b**). The response followed single-exponential behavior, with the observed rate k_{obs} of 0.88 ± 0.07 min^{-1} when measured at 15 °C (**Fig. 6c**). The value increased to 2.72 ± 0.38 min^{-1} when we raised the temperature to 20 °C (**Supplementary Fig. 5b**).

In our assays we initiated cleavage by the addition of Mg^{2+} at saturating concentrations of 10 mM. This concentration guarantees that folding of the ribozyme into the catalytically active conformation occurs almost instantaneously (in less than 1–2 s, corresponding to the immediate fluorescence decrease that is consistent with U26-Ap57 base pair formation; **Fig. 6b**).

DISCUSSION

The pistol ribozyme is unusual both in terms of its small size and limited secondary structure relative to other nucleolytic ribozymes. Thus, it remained to be discovered which features of its topology would facilitate site-specific self-cleavage at the G53-U54 site located within the short arm of the internal loop linking stems P2 and P3. We observed formation of the predicted pseudoknot[2], where it is embedded within the fold of the pistol ribozyme (**Fig. 1d**). The pseudoknot, together with its adjacent short noncanonical pairing segment, was positioned between flanking P1 and P3 stems (**Fig. 1c** and **Supplementary Fig. 1a**). Such coaxial stacking of helical segments (**Supplementary Fig. 1a**) is a common feature of higher-order RNA folds. Cleavage site residue G53 is part of this continuous helical stacking alignment (**Fig. 1c** and **Supplementary Fig. 1a**), while cleavage site residue U54 is displaced and stacks with G55 of outwardly directed stem P2 (**Fig. 1d**), thereby explaining the splayed-out alignment observed for the G53-U54 cleavage site.

A Mg^{2+} cation was bound proximal to the cleavage site in the fold of the pistol ribozyme (**Supplementary Fig. 1d**), but given that it was not directly coordinated to neither of the nonbridging phosphate oxygens at the G53-U54 cleavage site, it most likely contributes to electrostatic stabilization rather than catalysis. This result contrasts with the observation of a Mg^{2+} bound directly to the nonbridging phosphate oxygen at the cleavage site in the twister ribozyme[29,30].

The conserved residues in the pistol ribozyme[2,32] are dispersed between G5 in the stem-loop, A19-A20-A21 in the linker segment and A31-A32-G33 and G40-C41-G42 on opposite sides of the internal loop. They have key stabilizing and catalytic roles in the structure of the pistol ribozyme. Both G5 (**Supplementary Fig. 1c**) and G40, as well as C41 (**Fig. 2c**) participated in base triple formation, with G5 involved in stabilizing the junction between P1 and pseudoknot stems, while the G40 and C41 are involved in stabilizing the junction between pseudoknot and P3 stems bridged by the short noncanonical paired segment of the internal loop. Notably, both A31-A32-G33 and G40-C41-G42 segments were positioned in the proximity of the G53-U54 cleavage site (**Fig. 2a**), thereby sculpting the arrangement of nucleotides that surround the cleavage pocket. The A19-A20-A21 segment was positioned in the minor groove of stem P1, where it formed stabilizing twisted A-minor triple interactions (**Fig. 2d**,**e**). Conserved G40 and A32 were positioned to play key roles in catalyzing the cleavage chemistry (see below).

G42 appears to be important for proper positioning G40 and A32 bases as a consequence of formation of a hydrogen bond between its 2-NH_2 and A32 2′-O (2.7 Å), and additionally, between its O6 and G40 2-NH_2 (2.8 Å) and G53 2-NH_2 (2.7 Å) (**Fig. 2b**). This conclusion was supported by G42 mutation data (**Fig. 4g**,**i**).

We observed a splayed-apart arrangement at the G53-U54 cleavage site in the pistol ribozyme, with both G53 and U54 anchored in place by being sandwiched between flanking bases (**Fig. 3a**). Such extended splayed-apart alignments at the cleavage site has been reported previously for other nucleolytic ribozymes[1]. We observed a near in-line alignment (angle of 167°) at the G53-U54 cleavage site (**Fig. 3b**), similar to what we reported previously for the cleavage site in the twister ribozyme[29]. Such in-line alignments are a general feature critical for cleavage chemistry and have been reported for hammerhead[14] and hairpin[15,16] ribozymes.

The conserved G40 nucleotide was positioned proximal to the G53-U54 cleavage site in the structure of the pistol ribozyme (**Fig. 2a**) and anchored and aligned in place though base triple formation (**Fig. 2c**). G40 was the closest nucleotide to the modeled 2′-OH of

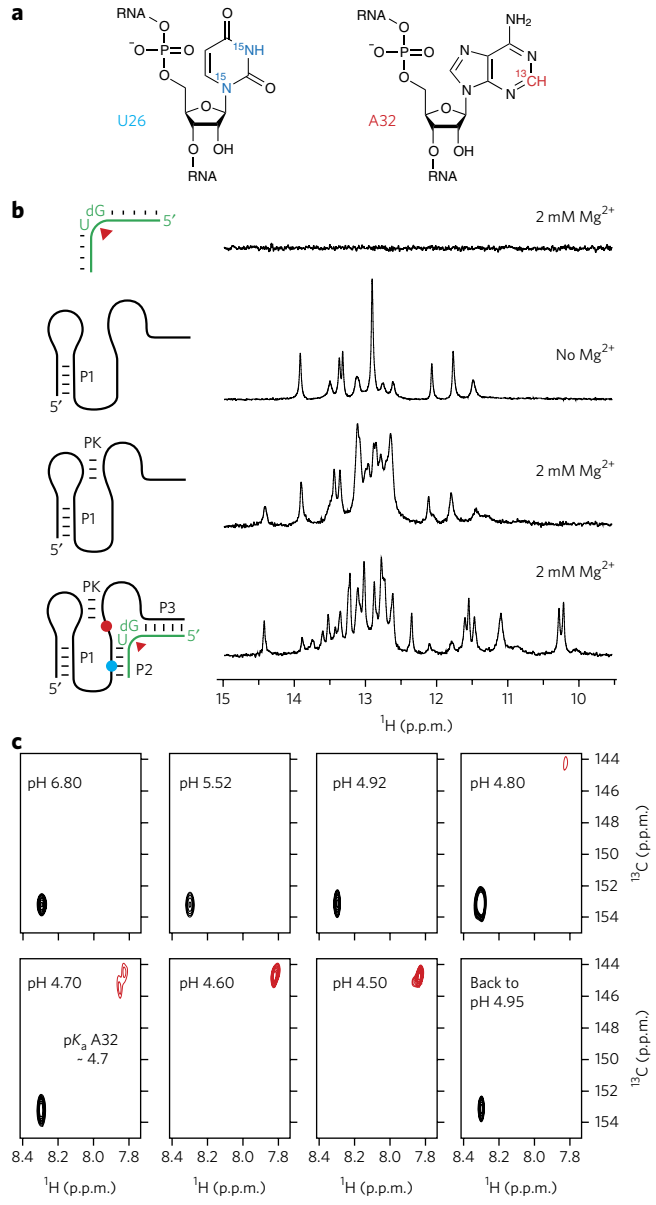

Figure 5 | NMR spectroscopic analysis of the env25 pistol ribozyme in solution. (**a**) Chemical structures of ^{15}N1/3-labeled U26 and ^{13}C2-labeled A32 used. (**b**) Complex formation verified by ^{1}H NMR imino proton spectroscopy; spectra assigned to cartoons of RNA strands used. (**c**) $^{1}J(^{1}H,^{13}C)$ HSQC spectra of the ^{13}C-A32 pistol complex at varying pH values. Conditions: c(RNA) = 80–120 µM; 25 mM NaCl, 2 mM $MgCl_2$, 15 mM sodium phosphate, H_2O/D_2O 9:1, 298 K.

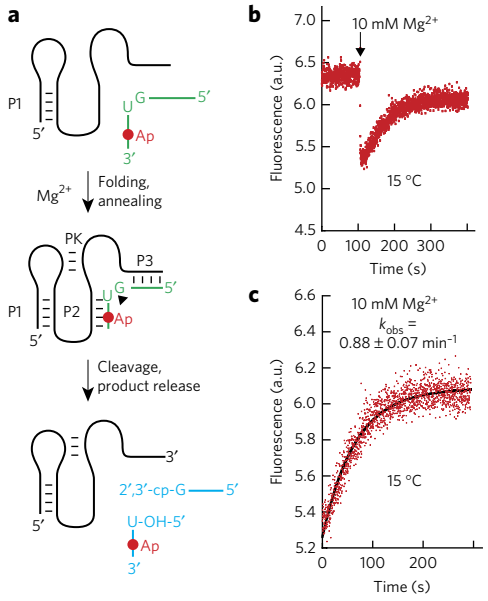

Figure 6 | Cleavage kinetics of the env25 pistol ribozyme analyzed by Ap fluorescence. (**a**) Schematics of the fluorescence assay that reports on folding and annealing, and cleavage product release. (**b**) Qualitative assay results showing fluorescence time course of the A57Ap variant upon $MgCl_2$ addition (black arrow); conditions: c(RNA) = 0.5 µM, 50 mM KMOPS, 100 mM KCl, 15 °C, pH 7.5; mixing was performed manually in less than 2 s resulting in 10 mM Mg^{2+} concentration. (**c**) Quantitative assay for rate determination at 15 °C based on data in **b**; arbitrary units (a.u.).

G53 at the G53-U54 cleavage site, with 3.4 Å separation between N1 of G40 and the 2′-OH oxygen of G53. We observed no cleavage for the G40A mutant (**Fig. 4b**), indicative of G40 being a strong candidate for the general base positioned to abstract the 2′-OH proton of G53, thereby impacting acid-base catalysis at the G53-U54 site in the pistol ribozyme.

The conserved A32 nucleotide was also positioned proximal to the G53-U54 cleavage site in the structure of the pistol ribozyme (**Fig. 2a**). A32 was anchored in place through hydrogen bond formation between its N7 atom and the base edge of U30 and between its 2′-OH and the 2-NH_2 group of G42 (**Fig. 2b**). A32 is the closest nucleotide to the bridging P-O5′ oxygen at the G53-U54 cleavage site, with separation between the P-O5′ oxygen, and the N3 and 2′-OH of A32 in the 5.0–5.3 Å range. Our results indicated that A32 is a strong candidate for a general acid during cleavage of the G53-U54 site, with contributions from both the base N3 atom and the ribose 2′-OH group.

Several lines of evidence support a role for N3 of A32 in the catalytic mechanism. Replacement of A32 by G had no impact on cleavage rate (**Supplementary Fig. 2d**), a result consistent with both purines having an N3 atom. By contrast, replacement by the smaller pyrimidines resulted either in no cleavage for the A32C variant (**Fig. 4c**) or reduced cleavage for the A32U variant (**Supplementary Fig. 2c**). Replacement of N3 by C3 resulted in no cleavage for the A32c3dA variant (**Fig. 4e**). In addition, the measured pK_a of 4.7 for A32 in the pistol ribozyme (**Fig. 5c**) shifted by one pK_a unit compared to the pK_a value of 3.6 for free adenosine[36] and 3.6–3.8 at the single-strand and duplex level (**Supplementary Fig. 4**). This shift in pK_a is comparable to the pK_a shift of 1.4 units reported previously for the adenine at the cleavage site of the twister ribozyme[30], consistent with participation of partially protonated A32 in phosphodiester cleavage chemistry.

Support for participation of the 2′-OH of A32 in cleavage chemistry is cemented by the reduced cleavage activity for the A32dA variant (**Fig. 4d**) relative to the wild-type pistol ribozyme (**Fig. 4a**). As we observed no cleavage for the A32c3dA variant (**Fig. 4e**) relative to partial cleavage observed for the A32dA variant (**Fig. 4d**), it appears that the N3 base position of A32 makes a larger contribution to catalysis than does the 2′-OH in the pistol ribozyme.

Our real-time fluorescence cleavage assay revealed kinetics for the pistol ribozyme (**Fig. 6**) that are consistent with previously reported rates in the range of 1–10 min^{-1} (refs. 2,32). Temperature had a considerable impact (**Fig. 6c** and **Supplementary Fig. 5b**), which likely correlates to multiple factors, including proper pseudoknot folding and substrate annealing, formation of the splayed out conformation of GpU, but also to release of the cleavage product. The obtained rates also compare well with the rates of other fast-cleaving ribozymes (for example, twister ribozyme

cleaves with 1.41 ± 0.16 min^{-1} at 15 °C and 2.44 ± 0.31 min^{-1} at 20 °C under the same conditions)[29]. We note that cleavage under single-turnover conditions proceeded in quantitative yield for the env25 pistol ribozyme; even a threefold excess of substrate resulted in complete cleavage consistent with multiple turnovers (**Fig. 4g**). This has not been observed for the previously investigated env22 twister ribozyme[29]; single-turnover conditions gave at most 80% cleavage, likely because of a more stably paired cleavage fragment that caused product inhibition (14-nt fragment with 10 base pairs formed in twister as opposed to 6-nt fragment with 5 base pairs formed in pistol)[29].

Recently, three crystal structures have been reported for the RzB hammerhead ribozyme, namely on crystals grown at pH 5.0 and 8.0 (ref. 37) and on a transition-state vanadate mimic[38]. These structural snapshots of the hammerhead ribozyme establish that the conformation centered about the cleavage site undergoes a substantial structural transition for crystals from pH 5.0 to 8.0, and a lesser transition for crystals from the pH 8.0 to the transition state vanadate mimic. These changes include repositioning of the putative general base (guanine) and a pair of divalent cations. We compared our structure of the env25 pistol ribozyme (**Fig. 3c**) with the pH 8.0 structure of the RzB hammerhead ribozyme (**Fig. 3d**) for the segments surrounding the cleavage site. For both ribozymes, the Watson-Crick edge of a guanine base is directed toward the to-be-abstracted 2′-OH proton, with the 2′-O positioned for in-line alignment relative to the to-be-cleaved P-O5′ bond (**Fig. 3c**,**d**). A divalent cation is coordinated to the O6 of the guanine (G12) in the hammerhead ribozyme (**Fig. 3d**), presumably with the potential to impact on its pK_a. The situation is different between the two ribozymes for residues aligning with the 5′-O at the cleavage site. The pistol ribozyme aligns an adenine (A32) whose N3 and 2′-OH are positioned toward the 5′-O at the cleavage site (**Fig. 3c**), thereby contributing to putative general acid catalysis. A similar alignment of an adenine N3 relative to the O-5′ oxygen has been observed in the twister ribozyme[28,29]. In addition, both ribozymes contain a hydrated divalent cation that makes outer-sphere coordination to the pro-R non-bridging phosphate oxygen, while being directly coordinated to the N7 of a guanine base (**Fig. 3c**,**d**). It has been proposed that the divalent cation-coordinated water ligand could serve as a general acid mediating catalysis in the hammerhead ribozyme[38]. It should be noted that a divalent cation was inner-sphere-coordinated to the nonbridging phosphate oxygen at the cleavage site in the twister ribozyme[29]. Further insights into the catalytic cleavage mechanism of nucleolytic ribozymes should emerge after comparison of transition-state vanadate mimics of pistol (not yet available) and hammerhead[38] ribozymes.

It is very likely that the structure of the pistol ribozyme reported in this study reflects a precatalytic ground-state conformation. We anticipate that formation of a catalytically cleavage-competent state will require small conformational transitions given that the distances between the N3 and 2′-OH of A32 and the O5′ oxygen at the cleavage site are in the 5 Å range (**Fig. 3c**), requiring bringing them closer together for the adenine (A32) to be effective as a putative general acid in the pistol ribozyme.

Received 9 March 2016; accepted 8 June 2016;
published online 11 July 2016

METHODS

Methods and any associated references are available in the online version of the paper.

Accession codes. Protein Data Bank (PDB): atomic coordinates and structure factors have been deposited under the following accession codes: 5K7C for dG53-containing env25 twister ribozyme, 5K7D for same ribozyme crystals bound to $Ir(NH_3)_6^{3+}Cl_3$ and 5K7E for same ribozyme crystals soaked in Mn^{2+}.

References

1. Jimenez, R.M., Polanco, J.A. & Luptak, A. Chemistry and biology of self-cleaving ribozymes. *Trends Biochem. Sci.* **40**, 648–661 (2015).
2. Weinberg, Z. *et al.* New classes of self-cleaving ribozymes revealed by comparative genomics analysis. *Nat. Chem. Biol.* **11**, 606–610 (2015).
3. Prody, G.A., Bakos, J.T., Buzayan, J.M., Schneider, I.R. & Bruening, G. Autolytic processing of dimeric plant virus satellite RNA. *Science* **231**, 1577–1580 (1986).
4. Hutchins, C.J., Rathjen, P.D., Forster, A.C. & Symons, R.H. Self-cleavage of plus and minus RNA transcripts of avocado sunblotch viroid. *Nucleic Acids Res.* **14**, 3627–3640 (1986).
5. Saville, B.J. & Collins, R.A. A site-specific self-cleavage reaction performed by a novel RNA in Neurospora mitochondria. *Cell* **61**, 685–696 (1990).
6. Perreault, J. *et al.* Identification of hammerhead ribozymes in all domains of life reveals novel structural variations. *PLOS Comput. Biol.* **7**, e1002031 (2011).
7. Webb, C.H., Riccitelli, N.J., Ruminski, D.J. & Luptak, A. Widespread occurrence of self-cleaving ribozymes. *Science* **326**, 953 (2009).
8. Buzayan, J.M., Gerlach, W.L. & Bruening, G. Non-enzymatic cleavage and ligation of RNAs complementary to a plant virus satellite RNA. *Nature* **323**, 349–353 (1986).
9. Fedor, M.J. Structure and function of the hairpin ribozyme. *J. Mol. Biol.* **297**, 269–291 (2000).
10. Winkler, W.C., Nahvi, A., Roth, A., Collins, J.A. & Breaker, R.R. Control of gene expression by a natural metabolite-responsive ribozyme. *Nature* **428**, 281–286 (2004).
11. Watson, P.Y. & Fedor, M.J. The ydaO motif is an ATP-sensing riboswitch in *Bacillus subtilis*. *Nat. Chem. Biol.* **8**, 963–965 (2012).
12. Webb, C.H. & Luptak, A. HDV-like self-cleaving ribozymes. *RNA Biol.* **8**, 719–727 (2011).
13. Lilley, D.M. The Varkud satellite ribozyme. *RNA* **10**, 151–158 (2004).
14. Martick, M. & Scott, W.G. Tertiary contacts distant from the active site prime a ribozyme for catalysis. *Cell* **126**, 309–320 (2006).
15. Rupert, P.B. & Ferre-D'Amare, A.R. Crystal structure of a hairpin ribozyme-inhibitor complex with implications for catalysis. *Nature* **410**, 780–786 (2001).
16. Rupert, P.B., Massey, A.P., Sigurdsson, S.T. & Ferre-D'Amare, A.R. Transition state stabilization by a catalytic RNA. *Science* **298**, 1421–1424 (2002).
17. Klein, D.J. & Ferre-D'Amare, A.R. Structural basis of glmS ribozyme activation by glucosamine-6-phosphate. *Science* **313**, 1752–1756 (2006).
18. Cochrane, J.C., Lipchock, S.V. & Strobel, S.A. Structural investigation of the GlmS ribozyme bound to Its catalytic cofactor. *Chem. Biol.* **14**, 97–105 (2007).
19. Ferré-D'Amaré, A.R., Zhou, K. & Doudna, J.A. Crystal structure of a hepatitis delta virus ribozyme. *Nature* **395**, 567–574 (1998).
20. Ke, A., Zhou, K., Ding, F., Cate, J.H. & Doudna, J.A. A conformational switch controls hepatitis delta virus ribozyme catalysis. *Nature* **429**, 201–205 (2004).
21. Suslov, N.B. *et al.* Crystal structure of the Varkud satellite ribozyme. *Nat. Chem. Biol.* **11**, 840–846 (2015).
22. Doherty, E.A. & Doudna, J.A. Ribozyme structures and mechanisms. *Annu. Rev. Biochem.* **69**, 597–615 (2000).
23. Cochrane, J.C. & Strobel, S.A. Catalytic strategies of self-cleaving ribozymes. *Acc. Chem. Res.* **41**, 1027–1035 (2008).
24. Ferré-D'Amaré, A.R. & Scott, W.G. Small self-cleaving ribozymes. *Cold Spring Harb. Perspect. Biol.* **2**, a003574 (2010).
25. Lilley, D.M. Mechanisms of RNA catalysis. *Phil. Trans. R. Soc. Lond. B* **366**, 2910–2917 (2011).
26. Roth, A. *et al.* A widespread self-cleaving ribozyme class is revealed by bioinformatics. *Nat. Chem. Biol.* **10**, 56–60 (2014).
27. Eiler, D., Wang, J. & Steitz, T.A. Structural basis for the fast self-cleavage reaction catalyzed by the twister ribozyme. *Proc. Natl. Acad. Sci. USA* **111**, 13028–13033 (2014).
28. Liu, Y., Wilson, T.J., McPhee, S.A. & Lilley, D.M. Crystal structure and mechanistic investigation of the twister ribozyme. *Nat. Chem. Biol.* **10**, 739–744 (2014).
29. Ren, A. *et al.* In-line alignment and Mg^{2+} coordination at the cleavage site of the env22 twister ribozyme. *Nat. Commun.* **5**, 5534 (2014).
30. Košutić, M. *et al.* A mini-twister variant and impact of residues/cations on the phosphodiester cleavage of this ribozyme class. *Angew. Chem. Int. Edn. Engl.* **54**, 15128–15133 (2015).
31. Gaines, C.S. & York, D.M. Ribozyme catalysis with a twist: active state of the twister ribozyme in solution predicted from molecular simulation. *J. Am. Chem. Soc.* **138**, 3058–3065 (2016).
32. Harris, K.A., Lunse, C.E., Li, S., Brewer, K.I. & Breaker, R.R. Biochemical analysis of pistol self-cleaving ribozymes. *RNA* **21**, 1852–1858 (2015).
33. Cai, Z. & Tinoco, I. Jr. Solution structure of loop A from the hairpin ribozyme from tobacco ringspot virus satellite. *Biochemistry* **35**, 6026–6036 (1996).

34. Kirk, S.R., Luedtke, N.W. & Tor, Y. 2-Aminopurine as a real-time probe of enzymatic cleavage and inhibition of hammerhead ribozymes. *Bioorg. Med. Chem.* **9**, 2295–2301 (2001).
35. Jeong, S., Sefcikova, J., Tinsley, R.A., Rueda, D. & Walter, N.G. Trans-acting hepatitis delta virus ribozyme: catalytic core and global structure are dependent on the 5′ substrate sequence. *Biochemistry* **42**, 7727–7740 (2003).
36. Kapinos, L.E., Operschall, B.P., Larsen, E. & Sigel, H. Understanding the acid-base properties of adenosine: the intrinsic basicities of N1, N3 and N7. *Chemistry* **17**, 8156–8164 (2011).
37. Mir, A. *et al.* Two divalent metal ions and conformational changes play roles in the hammerhead ribozyme cleavage reaction. *Biochemistry* **54**, 6369–6381 (2015).
38. Mir, A. & Golden, B.L. Two active site divalent ions in the crystal structure of the hammerhead ribozyme bound to a transition state analogue. *Biochemistry* **55**, 633–636 (2016).

Acknowledgments

We acknowledge assistance by staff at Northeastern Collaborative Access Team (NE-CAT) beamlines at the Advanced Photon Source and the experimental station 14-1 at the Stanford Synchrotron Radiation Light Source. X-ray diffraction studies were conducted at the Advanced Photon Source on the Northeastern Collaborative Access Team beamlines, which are supported by a grant from the National Institute of General Medical Sciences (P41 GM103403) from the US National Institutes of Health (NIH). Use of the Advanced Photon Source, an Office of Science User Facility operated for the US Department of Energy (DOE) Office of Science by Argonne National Laboratory, was supported by the US DOE under contract DE-AC02-06CH11357. A.R. was supported in part by new faculty start-up funds from Zhejiang University and the Thousand Young Talents Plan of China. The research was supported by US NIH grant 1 U19 CA179564 to D.J.P., by the Memorial Sloan-Kettering Cancer Center Core Grant (P30 CA008748), and the Austrian Science Fund FWF (P27947, I1040 to R.M., P26550, P28725 to C.K.), and the Swiss National Foundation SNF (Early Postdoc.Mobility to J.G.).

Author contributions

A.R. undertook all of the crystallographic experiments and the structure analysis with the assistance of P.G. under the supervision of D.J.P. while N.V., J.G. and M.J. were involved in nucleoside phosphoramidite synthesis, RNA preparation and cleavage assays under the supervision of R.M. C.K. designed and performed NMR spectroscopy measurements. The paper was written jointly by A.R., N.V., C.K., R.M. and D.J.P. with input from the remaining authors.

Competing financial interests

The authors declare no competing financial interests.

Additional information

Any supplementary information, chemical compound information and source data are available in the online version of the paper. Reprints and permissions information is available online at http://www.nature.com/reprints/index.html. Correspondence and request for materials should be addressed to D.J.P. or R.M.

ONLINE METHODS

Solid-phase synthesis of oligonucleotides. Standard phosphoramidite chemistry was applied for RNA solid-phase synthesis using 2′-*O*-TOM standard RNA nucleoside phosphoramidite building blocks (ChemGenes) and polystyrene support (GE Healthcare, Custom Primer Support, 80 µmol/g; PS 200). All oligonucleotides were synthesized on a ABI 392 Nucleic Acid Synthesizer following standard methods: detritylation (80 s) with dichloroacetic acid/1,2-dichloroethane (4/96); coupling (2.0 min) with phosphoramidites/acetonitrile (0.1 M x 130 µL) and benzylthiotetrazole/acetonitrile (0.3 M × 360 µL); capping (3 × 0.4 min, Cap A/Cap B = 1/1) with Cap A: 4-(dimethylamino)pyridine in acetonitrile (0.5 M) and Cap B: Ac_2O/sym-collidine/acetonitrile (2/3/5); oxidation (1.0 min) with I_2 (20 mM) in THF/pyridine/H_2O (35/10/5). The solutions of amidites and tetrazole, and acetonitrile were dried over activated molecular sieves (4 Å) overnight.

5′-*O*-(4,4′-dimethoxytrityl)-2′-deoxyguanosine phosphoramidite was purchased from ChemGenes. 5′-*O*-(4,4′-dimethoxytrityl)-3-deaza-2′-deoxyadenosine (c^3dA) phosphoramidite was synthesized according to reference 39 or purchased form GlenResearch. ^{13}C2-adenosine phosphoramidite was synthesized according to reference 40.

Deprotection of oligonucleotides. The solid support was treated each with $MeNH_2$ in EtOH (33%, 0.5 mL) and $MeNH_2$ in water (40%, 0.5 mL) for 7 h at room temperature. The supernatant was removed from and the solid support was washed 3 × with ethanol/water (1/1, v/v). The supernatant and the washings were combined with the deprotection solution of the residue and the whole mixture was evaporated to dryness. To remove the 2′-silyl protecting groups the resulting residue was treated with tetrabutylammonium fluoride trihydrate (TBAF·3H_2O) in THF (1 M, 1 mL) at 37 °C overnight. The reaction was quenched by the addition of triethylammonium acetate (TEAA) (1 M, pH 7.4, 1 mL). The volume of the solution was reduced and the solution was desalted with a size exclusion column (GE Healthcare, HiPrep 26/10 Desalting; 2.6 × 10 cm; Sephadex G25) eluting with H_2O, the collected fraction was evaporated to dryness and dissolved in 1 ml H_2O. Analysis of the crude RNA after deprotection was performed by anion-exchange chromatography on a Dionex DNAPac PA-100 column (4 mm × 250 mm) at 80 °C. Flow rate: 1 mL/min, eluant A: 25 mM Tris·HCl (pH 8.0), 6 M urea; eluant B: 25 mM Tris·HCl (pH 8.0), 0.5 M $NaClO_4$, 6 M urea; gradient: 0–60% B in A within 45 min or 0–40% B in 30 min for short sequences up to 15 nucleotides, UV detection at 260 nm.

Purification of RNA. Crude RNA products were purified on a semipreparative Dionex DNAPac PA-100 column (9 mm × 250 mm) at 80 °C with flow rate 2 ml/min. Fractions containing RNA were loaded on a C18 SepPak Plus cartridge (Waters/Millipore), washed with 0.1–0.15 M $(Et_3NH)^+HCO_3^-$, H_2O and eluted with H_2O/CH_3CN (1/1). RNA containing fractions were lyophilized. Analysis of the quality of purified RNA was performed by anion-exchange chromatography with same conditions as for crude RNA; the molecular weight was confirmed by LC-ESI mass spectrometry. Yield determination was performed by UV photometrical analysis of oligonucleotide solutions.

Mass spectroscopy of RNA. All experiments were performed on a Finnigan LCQ Advantage MAX ion trap instrumentation connected to an Amersham Ettan micro LC system. RNA sequences were analyzed in the negative-ion mode with a potential of -4 kV applied to the spray needle. LC: Sample (200 pmol RNA dissolved in 30 µL of 20 mM EDTA solution; average injection volume: 30 µL); column (Waters XTerraMS, C18 2.5 µm; 1.0 × 50 mm) at 21 °C; flow rate: 30 µL/min; eluant A: 8.6 mM TEA, 100 mM 1,1,1,3,3,3-hexafluoroisopropanol in H_2O (pH 8.0); eluant B: methanol; gradient: 0–100% B in A within 30 min; UV detection at 254 nm.

Crystallization. The sample for crystallization was generated by annealing the two purified strands of env25 pistol ribozyme at 70 °C for 3 min in a buffer containing 50 mM K-HEPES, pH 6.8, 100 mM KCl and 2 mM $MgCl_2$ followed by incubation at room temperature for 5 min and then cooling on ice for 30 min before setting up crystallization trials. To prevent the cleavage of the ribozyme during crystallization, G53 was replaced by deoxy-G in the substrate strand.

The crystals of the env25 pistol ribozyme were grown at 20 °C over a period of 2 weeks using the sitting-drop vapor diffusion approach after mixing the RNA at an equimolar ratio with the reservoir solution containing 0.1 M Na-cacodylate, pH 6.5, $Mg(OAc)_2$ 0.2 M and 32% MPD. For data collection, crystals were quickly flash-frozen in liquid nitrogen.

For $Ir(NH_3)_6^{3+}$ soaking experiments, crystals were transferred into the crystallization solution containing 0.1 M Na-cacodylate, pH 6.5, $Mg(OAc)_2$ 0.2 M and 32% MPD and supplemented with 5 mM $Ir(NH_3)_6^{3+}Cl_3$ at 4 °C for 24 h.

For Mn^{2+} soaking experiments, crystals were transferred into the crystallization solution containing 0.1 M Na-cacodylate, pH 6.5, 0.05 M $Mg(OAc)_2$ and 32% MPD and supplemented with 150 mM $MnCl_2$ at 4 °C for 24 h.

X-ray data collection and refinement. The $Ir(NH_3)_6^{3+}$ soaked crystals diffraction data were collected at 100K at beamline 14-1 located at the Stanford Synchrotron Radiation Light Source, using Rayonix Mx325 CCD detector. The native crytsal diffraction data were collected at 100K at NE-CAT beamline 24-ID-C located at the Advanced Photon Source, using Pilatus 6M detector. Data were processed using the HKL2000 (HKL Research) and XDS programs. The crystals belong to space group $P322_1$ (**Supplementary Table 1**). Based on the molecular weight of 20,400 Da, one molecule is expected per asymmetric unit with 55% solvent, which is typical for RNA molecules. Using the iridium SAD data, two iridium sites were located using SHELXC and SHELXD as implemented in HKL2MAP program[41]. These heavy atom sites were refined using the program PHASER. Iterations of model building, phase combination and density modification enabled us to build the complete model using PHENIX[42] and COOT[43]. The model was refined employing PHENIX using 2.7 Å native data set (**Supplementary Table 1**). Metal ions and their coordinated waters were identified based on 2*Fo* − *Fc* and *Fo* − *Fc* maps guided by the coordination geometries. Mg^{2+} sites were verified by soaking the crystal in Mn^{2+}-containing solution and collect the anomalous data set (**Supplementary Fig. 1e**). The X-ray data statistics of the native and iridium hexamine-containing and Mn^{2+}-containing crystals are listed in **Supplementary Table 1**.

Cleavage assays. Aliquots from aqueous millimolar stock solutions of the two RNA strands (R: ribozyme; S: substrate) were mixed and lyophilized. After addition of reaction buffer (30 mM HEPES, pH 7.5, 100 mM KCl, 2 mM $MgCl_2$) to yield a final concentration of c_{RNA} = 55 µM (each strand) in a total volume of 20 µL, the reaction was stopped by the addition of EDTA solution (20 µL; 3 mM) after 10, 45, and 120 min, stored at 4 °C, and subsequently analyzed by anion exchange HPLC (analytical Dionex DNAPac column) using the conditions as described above.

NMR spectroscopy experiments. All NMR spectra were recorded on a Bruker 600 MHz Avance II+ at 298 K equipped with a Prodigy TCI probe. One-dimensional ^{1}H NMR spectra were acquired with excitation sculpting for solvent suppression (Bruker pulse program: zgesgp), recording 512 scans. Two-dimensional ^{1}H-^{13}C-HSQC NMR spectra were recorded using a phase-sensitive ge-2D HSQC with water flip-back pulses and PEP with gradients in back-INEPT (Bruker pulse program hsqcetfpgpsi2): number of scans 72, spectral width in proton dimension 10 p.p.m., spectral width in carbon dimension 20 p.p.m., 2,048 × 32 complex data points, $^1J(^1H,^{13}C)$ = 200 Hz, interscan delay 1.0 s yielding an acquisition time of approx. 30 min per HSQC spectrum.

NMR spectroscopy sample preparation. The purified RNA (see above) was diluted with an equal volume of 100 mM sodium chloride solution and applied onto a C18 SepPak cartridge (Waters/Millipore). The cartridge was rinsed with water, followed by elution of the RNA with H_2O-acetonitrile 1:1. After lyophilization, the RNA sodium salt was dissolved in 420 µL NMR spectroscopy buffer (15 mM sodium phosphate, 25 mM sodium chloride in 9/1 H_2O/D_2O). Final pistol ribozyme RNA concentrations were between 80 µM and 120 µM. Magnesium chloride was added from a 1 M stock solution. The complex was formed by adding 1.2 equivalents of unlabeled substrate strand (with dG53 modification). Samples containing the bimolecular pistol complex were heated to 90 °C for two minutes and slowly cooled to room temperature to facilitate annealing of the two RNA strands.

For pH dependent experiments[44], the pH of the sample was determined directly in the 5 mm NMR spectroscopy tube using a Sigma-Aldrich micro

pH combination glass electrode and the pH was gradually adjusted by the addition of microliter amounts of 100 mM and 500 mM hydrochloric acid and 100/500 mM sodium hydroxide solutions, respectively. The pH of the solution was checked before and after the measurement. While the NMR spectrum was collected, the electrode was submerged in the pH 7 (for data between pH 6.8 and 5.5) or pH 4 (for data below pH 5.5) standard buffer.

Aminopurine fluorescence assays: cleavage kinetics. Rate constants k_{obs} for the A57Ap variant were measured under pseudo-first-order conditions with Mg^{2+} in excess over RNA. Stock solutions were prepared for the A57Ap variant (concentration of each strand c_{RNA} = 0.5 µM in 50 mM potassium 3-(*N*-morpholino) propanesulfonate (KMOPS), pH 7.5, 100 mM KCl) and for $MgCl_2$ (concentration c_{MgCl2} = 1.0 M in 50 mM KMOPS; 100 mM KCl pH 7.5). Mixing of 120 µl RNA stock solution and of 1.2 µl $MgCl_2$ stock solution manually, resulted in a final concentration of 0.5 µM RNA and 10 mM $MgCl_2$. Spectra were recorded on a Varian Cary Eclipse spectrometer at 15 °C and 20 °C (as indicated) using the following instrumental parameters: excitation wavelength, 308 nm; emission wavelength, 372 nm; increment of data point collection, 0.2 s; slit widths, 10 nm. The fluorescence data were fit to a single-exponential equation: $F = A_1 + A_2\, e^{-kt}$ (A_1: final fluorescence; $A_2\, e^{-kt}$: change in fluorescence over time (t) at the observed rate *k*'). The observed rate value provided is an arithmetic mean, determined from at least three independent measurements. All data processing was performed using *Kaleidagraph* software (Synergy Software).

39. Erlacher, M.D. *et al.* Efficient ribosomal peptidyl transfer critically relies on the presence of the ribose 2′-OH at A2451 of 23S rRNA. *J. Am. Chem. Soc.* **128**, 4453–4459 (2006).
40. Wunderlich, C. Advanced stable isotope labeling for NMR of RNA. PhD thesis, Leopold-Franzens University, Innsbruck, Austria (2015).
41. Schneider, T.P.T.R. HKL2MAP: a graphical user interface for phasing with SHELX programs. *J. Appl. Crystallogr.* **37**, 843–844 (2004).
42. Adams, P.D. *et al.* PHENIX: building new software for automated crystallographic structure determination. *Acta Crystallogr. D Biol. Crystallogr.* **58**, 1948–1954 (2002).
43. Emsley, P. & Cowtan, K. Coot: model-building tools for molecular graphics. *Acta Crystallogr. D Biol. Crystallogr.* **60**, 2126–2132 (2004).
44. Wilcox, J.L. & Bevilacqua, P.C. pKa shifting in double-stranded RNA is highly dependent upon nearest neighbors and bulge positioning. *Biochemistry* **52**, 7470–7476 (2013).

doi:10.1038/nchembio.2125